Geophys. J. Int. (2007) **169,** 789–794 doi: 10.1111/j.1365-246X.2007.3396.x

FAST TRACK PAPER

A new analytical solution estimating the flexural rigidity in the Central Andes

S. Wienecke,[1,*,†] C. Braitenberg[2] and H.-J. Götze[3,*]

[1] *Geological Survey of Norway, Leiv Eirikssons vei 39, 7491 Trondheim, Norway*
[2] *Department of Earth Sciences, University Trieste, Via Weiss 1, 34100 Trieste, Italy*
[3] *Institut für Geowissenschaften, Abtl. Geophysik, CAU Kiel, Otto Hahn Platz 1, 24118 Kiel, Germany*

Accepted 2007 February 9. Received 2007 February 7; in original form 2006 May 23

SUMMARY

We present a new 2-D analytical solution of the fourth-order differential equation, which describes the flexure of a thin elastic plate.

The new analytical solution allows the differential equation for an elastic plate to be solved for any irregular shaped topography with a high spatial resolution. We apply the new method to the Central Andes. The flexural rigidity distribution calculated by this technique correlates well with tectonic units and the location of fault zones, for example, the Central Andean Gravity High correlates with the presence of a rigid, high-density body.

Key words: crust, depth of compensation, gravity, isostasy, Moho discontinuity.

1 INTRODUCTION

The integration of geophysical, petrophysical and geological data allows the investigation of key processes of mountain building, the location of fault zones and the deformation processes within the crust. The spatial distribution of flexural rigidity indicates significant structural units of the crust as a function of their isostatic response. The flexural rigidity of the elastic lithosphere can be estimated using a fourth-order differential equation describing the flexure of a thin elastic plate (Turcotte & Schubert 1982; Göldner 1988). Hertz (1884) proposed three different solutions for the simple case of an ice plate floating on water. The deflection was calculated for a point load without taking the gravity into account. However, applied to geological problems the flexural values (in range of μm) were too small compared with the expected depths for a crust–mantle interface. For this reason spectral methods (coherence and admittance) have been preferred for the solution of the differential equation in the frequency space (Watts 1988). For continents, the reliability of the spectral technique has been questioned, because of drawbacks connected to the spectral approach (Braitenberg *et al.* 2002). The first drawback for the inverse calculation of the flexure from gravity observations is that the admittance method becomes unstable in the case of small topographic heights. Secondly, a large spatial window (at least 375-km side length) is required for the analysis (Macario *et al.* 1995). Even with new wavelet transform techniques using Forsyth's method (Swain & Kirby 2006) or methods which use a combination of admittance and coherence (Daly *et al.* 2004) such a side length is still necessary for higher flexural rigidity values. Accordingly the flexural rigidity distribution is estimated only roughly and correlation with smaller tectonic features not possible. Some of the disadvantages of the spectral methods were overcome by the convolution approach developed by Braitenberg *et al.* (2002). Although much work has been done to date, it is still questionable from the physical point of view, if it is sufficient to calculate the rigidity over an area of a side length lower than 375 km. The purpose of this study is to present a new analytical solution for an elastic plate (ASEP), making use of three solutions proposed by Hertz (1884). We evaluate all three solutions for their feasibility. The ASEP will be compared with the inverse Fourier transform of the transfer function of the spectral methods (Watts 2001), as both solve the same differential equation. As a case example for the application of the ASEP, we calculate the flexural rigidity distribution for the Central Andes, where an extensive database is available to us. We aim to establish our new method for calculating the flexural rigidity distribution with a high spatial resolution in order to compare the results with geological information.

2 METHOD

The new analytical solution solves the differential equation of the fourth order for any irregular shape of the topography. The equation, which was analytical solved, calculates the flexure w of a thin elastic plate:

*Formerly at: Institut für Geologische Wissenschaften, Fachbereich: Geophysik, Freie Universität Berlin, Malteserstr. 74–100, 12449 Berlin, Germany.
†Now at: Statoil Research Centre, Arkitekt Ebbellsvei 10, Rotvoll, N-7005 Trondheim, Norway. E-mail: suw@statoil.com.

$$\Delta \cdot \Delta w + \frac{1}{\beta^4} w = 0, \tag{1}$$

with Δ as the Laplace operator, which can be written in Cartesian coordinates: $\Delta = \frac{\partial^2}{\partial x^2} + \frac{\partial^2}{\partial y^2}$. The flexure parameter β is related to the flexural rigidity D by:

$$\beta = \sqrt[4]{\frac{D}{(\rho_m - \rho_c)g}} = \sqrt[4]{\frac{E T_e^3}{12(1-\nu^2)} \frac{1}{(\rho_m - \rho_c)g}}, \tag{2}$$

where ρ_m and ρ_c are the densities of the mantle and the crust, g is the acceleration due to the gravity, ν is Poisson's ratio, E is Young's modulus and T_e is the elastic thickness. The density ρ_i of the material that infills the flexural depression is assumed to be equal to the crustal density ρ_c. The set of three solutions proposed by Hertz (1884) was modified in order to apply it to the elastic lithosphere. The first solution is in the point of origin of the coordinate system, where the point load P acts. The deflection w_0 is expressed by Wienecke (2006):

$$w_0 = \frac{P}{8(\rho_m - \rho_c)g\beta^2}. \tag{3}$$

The formula describes the maximum depth of the deflection. For the second solution results (Watts 2001):

$$w(x,y) = \frac{P}{2\pi\beta^2(\rho_m - \rho_c)g} \times \left\{ \begin{array}{l} \frac{(r_{x,y})^2}{2^2} \cdot \ln(r_{x,y}) - \frac{(r_{x,y})^6}{2^2 \cdot 4^2 \cdot 6^2} \cdot \left(\ln(r_{x,y}) - \frac{5}{6} \right) + \cdots \\ + \frac{\pi}{4} \left(1 - \frac{(r_{x,y})^4}{2^2 \cdot 4^2} + \frac{(r_{x,y})^8}{2^2 \cdot 4^2 \cdot 6^2 \cdot 8^2} - \cdots \right) \\ \cdots - 1.1159 \cdot \left(\frac{(r_{x,y})^2}{2^2} - \frac{(r_{x,y})^6}{2^2 \cdot 4^2 \cdot 6^2} + \cdots \right) \end{array} \right\}. \tag{4}$$

We will call this solution 'logarithm function'. The radius $r_{x,y}$ is the normalised radial distance from the point of origin with:

$$r_{x,y} = \frac{\sqrt{x^2 + y^2}}{\beta}. \tag{5}$$

We will use also a third solution for the deflection (Wienecke 2006):

$$w(x,y) = \frac{P}{2\pi\beta^2(\rho_m - \rho_c)g} \sqrt{\frac{\pi}{2}} \frac{e^{-(r_{x,y})\sqrt{1/2}}}{\sqrt{(r_{x,y})}} \times \left\{ \sin\left[(r_{x,y}) \sqrt{\frac{1}{2}} + \frac{\pi}{8} \right] - \frac{1}{8(r_{x,y})} \sin\left[(r_{x,y}) \sqrt{\frac{1}{2}} + \frac{3\pi}{8} \right] + \cdots \right\}. \tag{6}$$

This solution is called 'sine function'. All three functions are composed to retrieve one analytical solution for the computation of the flexural rigidity (Fig. 1). Investigations show that the logarithm function is only valid for small values of the radius $r_{x,y}$. On the other hand the values for the deflection produced by the sine function are underestimated for smaller values of the radius $r_{x,y}$. The new analytical solution for an elastic plate (ASEP) by Wienecke (2006) is composed of all three functions and changes from the logarithm function into the sine function at a distance $r(x,y) = 2\beta$, since at this point both functions have the same deflection value (see Fig. 1).

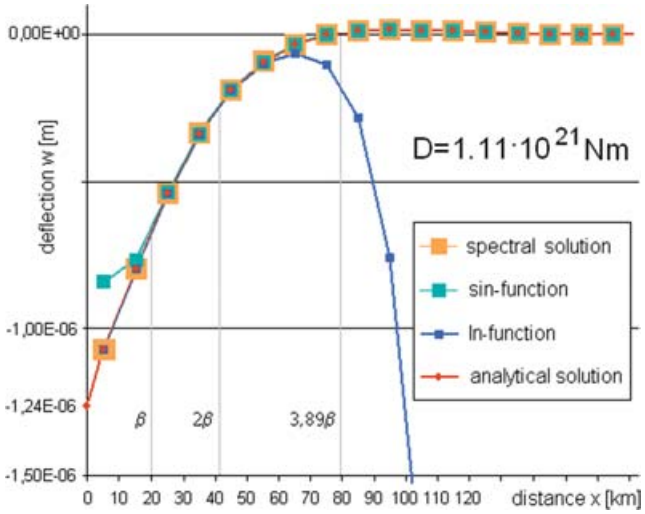

Figure 1. As example the analytical solution for an elastic plate (ASEP) is calculated for a point load with $h = 1$ km, $D = 1.11 \cdot 10^{21}$ Nm, $g = 9.81$ m s^{-2}, and the densities $\rho_m = 3350$ kg m^{-3} and $\rho_c = 2700$ kg m^{-3}. The ASEP consist of three different solutions in dependence of β: (a) solution for the point of origin, (b) sine and (c) logarithm function. The solutions are shown on a profile in the x-direction (therefore, r (x, y) corresponds to x in this case). Since at the point 2β the sine and logarithm functions have the same deflection value w, the ASEP consist of a logarithm function for the close range for all $r(x, y) \leq 2\beta$ and then changes to a sine function for the wide range for all $r(x, y) > 2\beta$. The ASEP (red colour) is in a very good agreement with the spectral solution (orange colour).

In spectral methods the differential equation (eq. 1) was solved with the fast Fourier transformation (FFT) using a transfer function according to the Vening–Meinesz approach. If we set the density of the material that infills the flexural depression ρ_i equal to the crustal density ρ_c, the transfer function Φ_δ for the wave number k is given by:

$$\Phi_\delta(k) = \frac{\rho_c}{\rho_m - \rho_c} \left[\frac{Dk^4}{(\rho_m - \rho_c)g} + 1 \right]^{-1}. \tag{7}$$

The spectral solution for a point load in the space domain is the inverse Fourier transformation of the transfer function (eq. 7). The comparison of the ASEP with the spectral solution for a point load shows a very good agreement between both solutions.

In order to apply the ASEP on a real topography we use the convolution approach as described by Braitenberg *et al.* (2006). For each grid node of the topographical input grid a flexure curve is calculated with the ASEP. Each grid node is defined by (x, y) coordinate pairs and a height (z). This height is used, with the density and the acceleration due to the gravity g, to define the point load. Each grid value is, in essence, a distributed 'rectangular' load. However, a point load is a rectangular load related to a unit area. Thus, the ASEP has to be 'normalized' to each grid node value by taking the area $A = \mathrm{d}x \cdot \mathrm{d}y$ into account, where $\mathrm{d}x$ is the grid node distance in x-direction and $\mathrm{d}y$ is the grid node distance in y-direction, respectively. This method was described and tested by Wienecke (2006). The superposition of all flexure curves defined by convolution provides the flexure crust–mantle interface (CMI). The comparison for a CMI calculated with the spectral method (eq. 7) and the ASEP is in a very good agreement (Wienecke 2006). The flexure CMI is calculated with the ASEP as a function of flexural rigidity. In view of the precision of the calculation and in order to avoid edge effects the area of the input topography is required to be larger than the

area of the computed flexure CMI by the amount of the radius of convolution. The convolution radius can be directly calculated as a function of the flexure parameter β (Wienecke 2006), and therefore, also as a function of rigidity and density contrast (e.g. for a rigidity $D = 8.89 \times 10^{18}$ Nm is the radius of convolution $R = 24$ km and for $D = 7.11 \times 10^{23}$ Nm is $R = 225$ km. This means that the calculated flexure CMI will be 225 km smaller than the topography at each side).

We compute a set of flexure CMIs for a range of rigidity values $D = 8.89 \times 10^{18}$ Nm till 2.44×10^{24} Nm, which corresponds, for the Poisson ration $\nu = 0.25$ and the Young's modulus $E = 100$ GPa, to the elastic thickness values $T_e = 1$ km till 65 km (see eq. 2).

Thus the flexure CMI corresponds exactly to one flexural rigidity value. Hence, the comparison of the computed flexure CMIs with a reference CMI (e.g. derived from 3-D density models) over an area with a given side length L provides one constant rigidity value for this subsection, resulting in a high spatial resolution of the 2-D flexural rigidity distribution.

The comparison of the flexure CMIs with a reference CMI is done by the choice of the minimum root mean square value (Braitenberg *et al*. 2006). For the reference CMI we make use of the gravity CMI, which was derived by Tassara (2006) using a 3-D density model.

3 APPLICATION TO CENTRAL ANDES

Our methodology has been applied to the Central Andes (15°S–33°S). Since 1993 the members of the collaborative research program 267 'Deformation processes in the Andes' have established a broad scientific data basis aiming to identify the key processes controlling the orogeny and plateau development in the Central Andes (Reutter *et al.* 1994; Götze & Migra-Group 1996; SFB267 2002). A main feature in this area is the Central Andean Gravity High (CAGH), which is limited in the west by the pre-cordilleran fault system and in the east by the Ocloyic fold and thrust belt (Fig. 2). The gravity signature of large amounts of Ordovician basic intrusive is one possible explanation for the CAGH (Götze & Kirchner 1997). The meaning of the CAGH was discussed in view of its evolution and structure (Bahlburg & Herve 1997; Götze & Krause 2002) and it was suggested that the anomalous masses causing the CAGH have played a major role in the tectonic development of the Andean region. The CAGH corresponds to a seismic high-velocity zone located at shallower depths (Lessel 1998; Lucassen *et al.* 1999; Haberland *et al.* 2003). Studies the gravity anomalies of the CAGH indicate a 400 km long and 100–400 km wide high-density body at 15 km depth (Götze & Krause 2002).

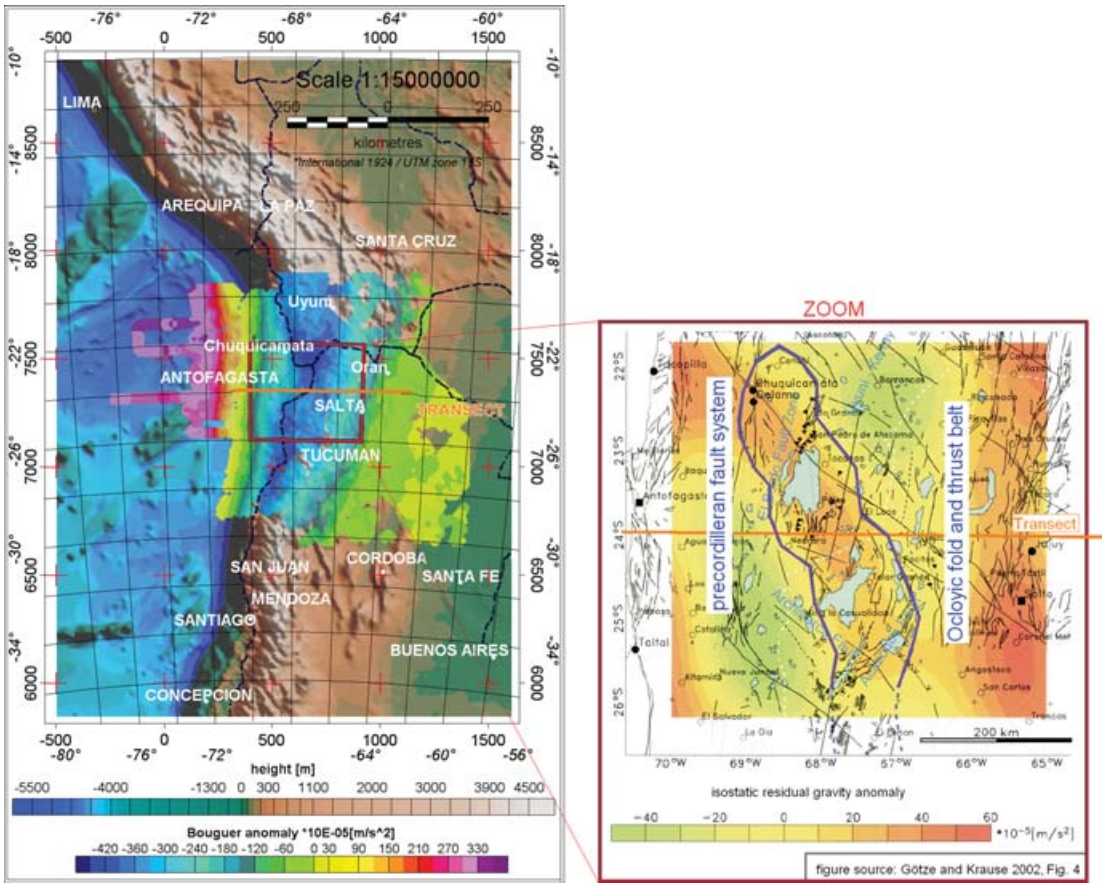

Figure 2. Topography of Central Andes with overlain Bouguer gravity and the main tectonic features. The red box shows the approximate location of the study area. The orange line shows the location of the cross section. The Central Andean Gravity High (CAGH) is located in the middle of the towns Antofagasta, Salta and Tucumán. Because of a similar observed topography compared to the surrounded area a much lower Bouguer gravity is expected. That is one reason why it is called 'High'. The other reason is, that it corresponds to a positive isostatic gravity anomaly (Vening Meinesz isostasy). On the left side the outlines of the CAGH are shown (violet coloured) as it is observed in the low pass filtered isostatic residual gravity field (figure source: Götze & Krause 2002).

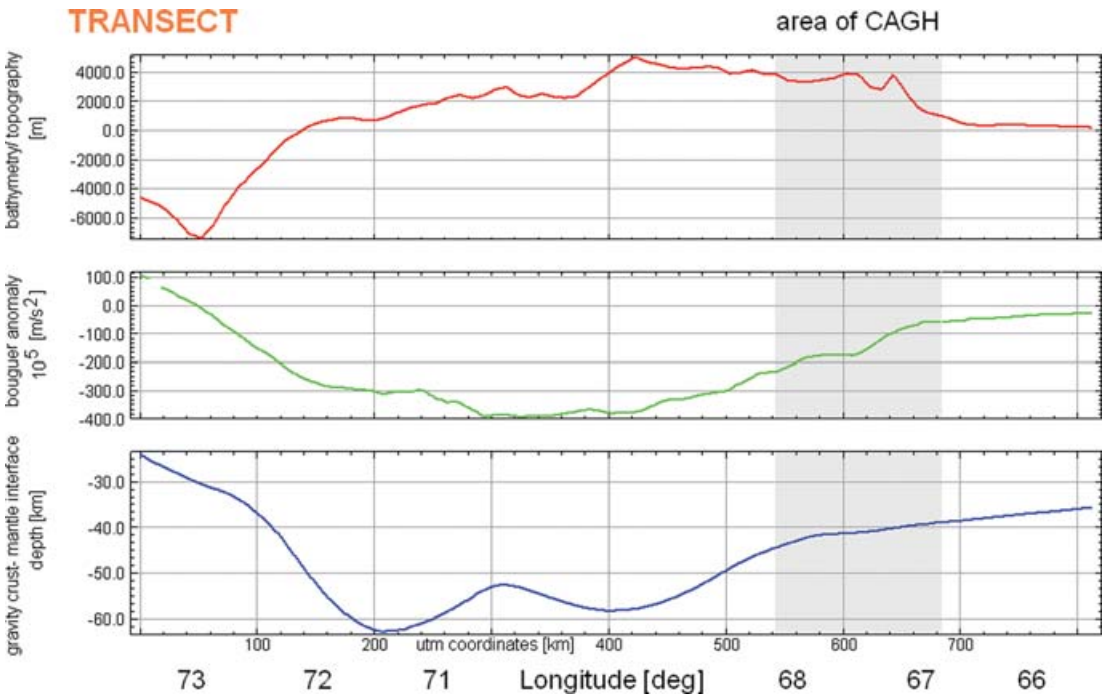

Figure 3. Cross-section of topography, Bouguer anomaly and the depth of the gravity crust–mantle interface (CMI) through the study area. In the area of the CAGH (68°W–67°W), which is coloured in grey, the observed topography is similar compared to the surrounded area (69°W–69°W), but the depths of the gravity CMI are much shallower. Because, given similar surface loading the crustal structure differs, we suggest that a higher flexural rigidity could explain the shallower gravity CMI and, therefore, the observed Bouguer gravity anomalies.

3.1 Data

Gravity data of the Central Andes were collected by field measurements and offshore shipboard campaigns (Götze *et al.* 1990). Tassara (2006) constructed a 3-D density model on this database using the modelling software IGMAS (Götze & Schmidt 1998). The density model provides information about depth, density contrast and undulation of the CMI, which are important input parameters for calculating the flexural rigidity.

A topographic cross-section through the study area (Fig. 3) shows the predicted crustal structure due to the 3-D gravity modelling (Tassara 2006). In the area of the CAGH (*ca.* 68°W–67°W), which is coloured in grey, we observe similar topography compare to the surroundings (*ca*. 69°W–68°W) and assume, therefore, similar surface loading. However, the predicted crustal structure from the observed Bouguer anomaly differs. We suggest that spatially varying of the flexural rigidity could explain the observed Bouguer gravity anomalies.

The topography/bathymetry from GEBCO (NGDC/NOAA 2003) was transformed to a 'model topography', which means that every point of the input grid with a height coordinate $z < 0$ was multiplied with the factor $\frac{(\rho_c - \rho_w)}{\rho_c} = 0.645$ for an assumed average density of the crust $\rho_c = 2900\,\mathrm{kg\,m^{-3}}$ and a density of water $\rho_w = 1030\,\mathrm{kg\,m^{-3}}$. This model topography was used as input grid for the calculation of flexure CMIs. The flexure is computed with the analytical solution for each grid node with a reference depth of 30 km, same density of crust and a mantle density of $\rho_m = 3380\ \mathrm{kg\ m^{-3}}$. The choice of these parameters is constrained by the average values of the density model. The reference depth corresponds theoretically to the crustal plate thickness, when no load is applied or to which deflection value the solution should converge in a case of infinitely high flexural rigidity (Wienecke 2006).

3.2 Distribution of flexural rigidity

The flexural rigidity distribution was calculated for subsections, which are squares with a side length of $L = 60$ km. The flexural rigidity is often expressed by the elastic thickness (eq. 2) assuming a constant Young's modulus of $E = 100$ GPa and a Poisson ratio $\nu = 0.25$ (Burov & Diament 1995).

Fig. 4 shows the elastic thickness distribution and location of lineaments, salt lakes and the CAGH (Reutter *et al.* 1994; Götze & Krause 2002; SFB267 2002). The Andean mountain belt is characterized by an area of low rigidity values, which indicates a weak crust (or a weak mantle, respectively). This result is in very good agreement with the geological studies suggesting a softening of the mountain belt due to fluid and melt associated processes driven by the subduction (SFB267 2002).

The location of the CAGH correlates with the presence of a rigid body compared to the surrounding area (yellow coloured in Fig. 4), which agrees with the observed high seismic velocities (Schurr 2001). High elastic thickness values are further estimated for the Brazilian shield. A very good correlation is observed between the direction and the location of faults and areas of rapid changes in the elastic thickness (from low to higher values). The Archibarca fault and the Calama–Olacapato–El Toro lineament (Fig. 4) are located between the borders of zones of high and low elastic thickness. Also the direction of the Atacama fault zone, the pre-cordilleran fault systems and the Ocloyic fold and thrust belt correlate well with the flexural rigidity distribution.

4 DISCUSSION

This method bears the advantage that, first, the flexure CMI is computed for the entire size of the study area and then—in a second

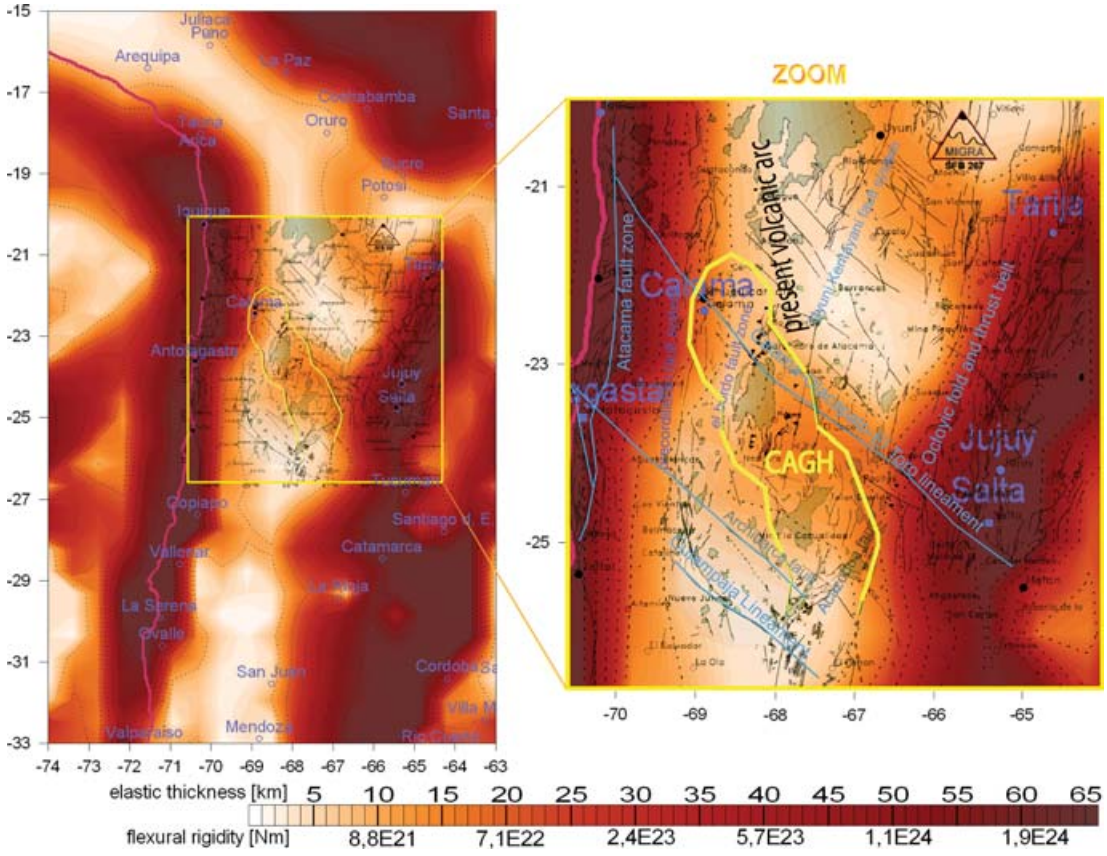

Figure 4. The rigidity distribution are overlain with geological lineaments, salt lakes and outline of CAGH in yellow (Götze & Krause 2002).

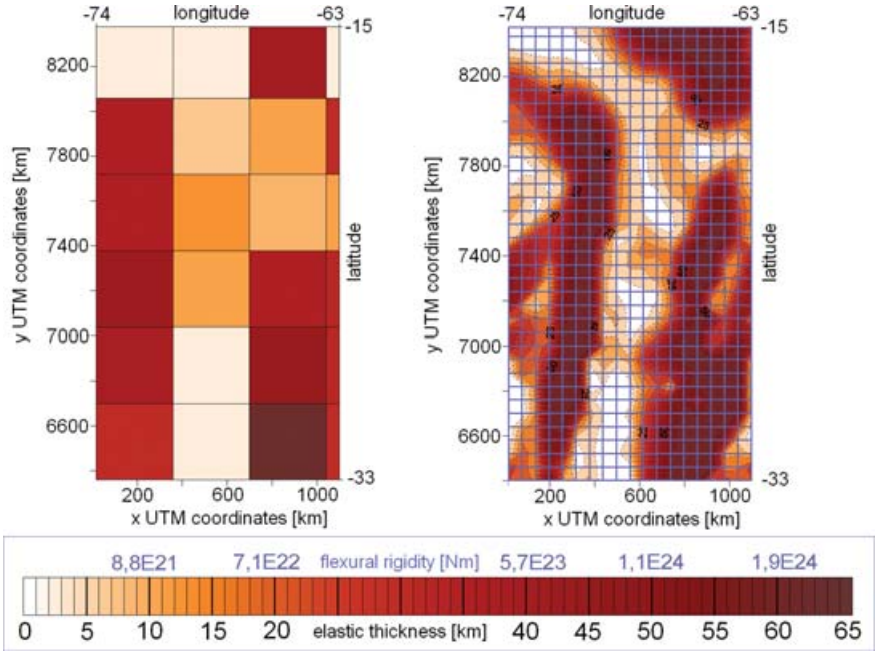

Figure 5. Rigidity distribution of Central Andes for different side lengths of subsections: 340 km (left side) and 60 km (right side).

step—the flexural rigidity is estimated by comparison of this flexure CMI with a reference CMI over a smaller subsection. Furthermore, the ASEP provides a solution for the point of origin, where the point load acts (Fig. 1). Therefore, the side length of the subsections can be chosen arbitrarily and consequently also the flexural rigidity is resolved with high resolution. Because of the high spatial resolution of the ASEP, a correlation with local tectonic features and faults can be obtained. In the admittance calculations the topographical input

stands in the denominator, therefore, the methods become unstable in case of small topography, while the analytical solution can be applied for any arbitrary small topographical input.

The good correlation between the flexural rigidity distribution pattern and the tectonic features indicates that we are able to resolve different deformation patterns. This means that we can predict tectonic units expressed by changes in flexural rigidity in areas where the geological information is not available. Due to its simplicity the method is applicable on study areas where only few information are accessible.

The analytical function is based on the assumption of a plate of constant thickness and variable thickness would require solving the asymmetric analytical function. Furthermore, the solution would be dependent on the size of the analysis window due to its asymmetry. However, the analysis applying different window sizes shows that our results are independent of the side length L of the subsections (Fig. 5). We compare the results of the flexural rigidity distribution calculated with a grid size $L = 340$ and 60 km. We observe, that the smaller grid size increases the resolution of the flexural rigidity calculation, but leads not to different results. The results of the rigidity distribution converge to each other. Uncertainties connected to input data are certainly more substantial than the deviation between the symmetric and asymmetric solution.

In this paper the subsurface loads were only taken into account via the reference CMI, which was derived with 3-D gravity modelling by Tassara (2006). In this paper the eqs 2–4 are shown for a point load P. The ASEP can be applied for surface, subsurface or combined loading, which was done and tested by Wienecke (2006). Therefore, the input grid contains the information about the topographic load, the subsurface load or the combined load, respectively. Our method bases on the thin elastic plate approximation and dependency on time and temperature are not yet considered. In the analytical case the quantities and influence of the input parameters and the interrelationship among these can be recognized. This is an important task for future work.

ACKNOWLEDGMENT

We acknowledge support from the SFB267 and DFG. S. Wienecke profited from the Socrates student exchange program between the University of Trieste and the Freie Universität Berlin. A. Nogeitzig, L. Gernigon and J. Ebbing are thanked for fruitful discussions. J. F. Kirby and an unknown reviewer are thanked for very useful comments and suggestions.

REFERENCES

Bahlburg, H. & Herve, F., 1997. Geodynamic evolution and tectonostratigraphic terranes of northwestern Argentina and northern Chile, *Geol. Soc. Am. Bull.,* **109,** 869–884.

Braitenberg, C., Ebbing, J. & Götze, H.J., 2002. Inverse modelling of elastic thickness by convolution method–the eastern Alps as a case example, *Earth Planet. Sci. Lett.,* **202,** 387–404.

Braitenberg, C., Wienecke, S. & Wang, Y., 2006. Basement structures from Satellite Derived Gravity Field: the South China Sea Ridge, *J. Geophys. Res.-Solid Earth,* **111,** B05 407, doi:10.1029/2005JB003938.

Burov, E.B. & Diament, M., 1995. The effective elastic thickness (T-E) of continental lithosphere—what does it really mean, *J. Geophys. Res.-Solid Earth,* **100,** 3905–3927.

Daly, E., Brown, C., Stark, C.P. & Ebinger, C.J., 2004. Wavelet and multitaper coherence methods for assessing the elastic thickness of the Irish Atlantic margin, *Geophys. J. Int.,* **159,** 445–459.

Göldner, H., 1988. *Leitfaden der technischen Mechanik: Statik, Festigkeitslehre, Kinematik, Dynamik,* Steinkopff Verlag, Darmstadt.

Götze, H.-J. & Kirchner, A., 1997. Interpretation of gravity and geoid in the Central Andes between 20 degrees and 29 degrees S, *J. South Am. Earth Sci.,* **10,** 179–188.

Götze, H.-J. & Krause, S. , 2002. The Central Andean gravity high, a relic of an old subduction complex?. *J. South Am. Earth Sci.,* **14,** 799–811.

Götze, H.J. & Migra-Group, 1996. Group updates the gravity database in the Central Andes (20°–29° S), *Eos Trans.,* AGU, **77,** 181–181, doi: 10.1029/96EO00122.

Götze, H.J. & Schmidt, S., 1998. Modeling techniques in geology and geophysics by the aid of geoscientific information systems (GIS), *Phys. Chem. Earth,* **23,** 86.

Götze, H.-J., Lahmeyer, B., Schmidt, S., Strunk, S. & Araneda, A., 1990. A new gravity data base in the central Andes (20°–26° S), *EOS Trans., AGU,* **71,** 401.

Haberland, C., Rietbrock, A., Schurr, B. & Brasse, H., 2003. Coincident anomalies of seismic attenuation and electrical resistivity beneath the southern Bolivian Altiplano plateau, *Geophys. Res. Lett.,* **30**(18), 1923, doi:10.1029/2003GL017492.

Hertz, H., 1884. Über das Gleichgewicht schwimmender elasticher Platten, *Ann. Phys. Chem.,* **22,** 449–455.

Lessel, K., 1998. Die Krustenstruktur der Zentralen Anden in Nordchile (21–24° S), abgeleitet aus 3D-Modellierung refraktionsseismischer Daten, *PHD thesis,* Free University of Berlin, Berlin.

Lucassen, F., Franz, G. & Laber, A., 1999. Permian high pressure rocks – the basement of the Sierra de Limon Verde in Northern Chile, *J. South Am. Earth Sci.,* **12,** 183–199.

Macario, A., Malinverno, A. & Haxby, W.F., 1995. On the robustness of elastic thickness estimates obtained using the coherence method, *J. Geophys. Res.-Solid Earth,* **100,** 151 63—15 172.

NGDC/NOAA, 2003. *General Bathymetric Chart of the Oceans (GEBCO),* ed. National Geophysical Data Center (NGDC), Boulder, CO.

Reutter, K.-J., Scheuber, E. & Wigger, P., 1994. *Tectonics of the Southern Central Andes,* p. 333, Springer-Verlag, Heidelberg.

Schurr, B., 2001. Seismic Structure of the Central Andean Subduction Zone from Local Earthquake Data, *PhD thesis,* Free University Berlin, Berlin.

SFB267, 2002. Interaction between endogenic and exogenic processes during subduction orogenesis, pp. http://sfb267.geoinf.fu-berlin.de/, edited, Collaborative Research Center, Berlin, Potsdam.

Swain, C.J. & Kirby, J.F., 2006. An effective elastic thickness map of Australia from wavelet transforms of gravity and topography using Forsyth's method, *Geophys. Res. Lett.,* **33,** L02 314, doi:10.1029/2005GL025090.

Tassara, A., 2006. Structure of the Andean continental margin and causes of its segmentation, *PhD thesis,* Free University of Berlin, Berlin, http://www.diss.fu-berlin.de/2005/330/index.html.

Turcotte, D.L. & Schubert, G., 1982. *Geodynamics: Applications of Continuum Physics to Geological Problems,* John Wiley and Sons, New York.

Watts, A.B., 1988. Gravity-anomalies, crustal structure and flexure of the lithosphere at the baltimore canyon trough, *Earth Planet. Sci. Lett.,* **89,** 221–238.

Watts, A.B., 2001. *Isostasy and Flexure of the Lithosphere*, Cambridge University Press, New York.

Wienecke, S., 2006. A new analytical solution for the calculation of flexural rigidity: significance and applications, *PhD thesis,* Free University of Berlin, Berlin, http://www.diss.fu-berlin.de/2006/42